Nature of heterointerfaces in GaAs/InAs and InAs/GaAs axial nanowire heterostructures

Mohanchand Paladugu,[1] Jin Zou,[1,2,a)] Ya-Nan Guo,[1] Xin Zhang,[1] Yong Kim,[3] Hannah J. Joyce,[4] Qiang Gao,[4] H. Hoe Tan,[4] and C. Jagadish[4,a)]
[1]*School of Engineering, The University of Queensland, St. Lucia, QLD 4072 Australia*
[2]*Centre for Microscopy and Microanalysis, The University of Queensland, St. Lucia QLD 4072, Australia*
[3]*Department of Physics, Dong-A University, Hadan-2-dong, Sahagu, Busan 604-714, Republic of Korea*
[4]*Department of Electronic Materials Engineering, Research School of Physical Sciences and Engineering, The Australian National University, Canberra ACT 0200, Australia*

(Received 7 July 2008; accepted 17 August 2008; published online 11 September 2008)

The structural and compositional characteristics of heterointerfaces of Au-catalyzed GaAs/InAs and InAs/GaAs axial nanowire heterostructures were comprehensively investigated by transmission electron microscopy. It has been found that the GaAs/InAs interface is not sharp and contains an InGaAs transition segment, and in contrast, the InAs/GaAs interface is atomically sharp. This difference in the nature of heterointerfaces can be attributed to the difference in the affinity of the group III elements with the catalyst material. © *2008 American Institute of Physics*.
[DOI: 10.1063/1.2978959]

Semiconductor nanowires (NWs) are promising one-dimensional (1D) nanostructures due to their potential applications in nanoscale electronic and optoelectronic devices.[1–3] These 1D nanostructures are generally induced by the vapor-liquid-solid (VLS) mechanism using metallic nanoparticles such as Au.[4,5] Heterogeneous nucleation of a solid from a liquid metal is a well studied process in which the solid nucleates preferentially on the solid surface of a nucleant. This nucleation of the solid is a function of the interfacial energies between the liquid metal and the nucleant and between the liquid metal and the nucleating solid.[6] According to this phenomenon, the nucleation of a NW is a function of the interfacial energies between the catalyst droplet and the underlying substrate and between the catalyst droplet and the nucleating NW.[7–9]

For axial NW heterostructures to be practically useful in device applications, it is essential to eliminate misfit dislocations at the strained heterointerface and to achieve sharp heterointerfaces. Although it is possible to eliminate misfit dislocations at the heterointerface of the axial NW heterostructures,[10] securing a sharp heterointerface has been a challenging task.[11] This issue is prominent especially because the materials from the vapor phase diffuse through the catalysts.[11] For this reason, a thorough understanding of the nature of heterointerfaces, in terms of their atomic structure and composition and the evolution of NW heterointerfaces, is essential for the growth of axial NW heterostructures with the desired properties. In this regard, we choose GaAs/InAs and InAs/GaAs NW heterostructures to study the nature of their heterointerfaces. The choice of this combination is also because only group III elements are known to diffuse through the catalysts (As does not alloy with the Au catalysts).[12] The details of heterointerface with a change in the group-III element should provide insight into NW growth and the role of the nanosized catalyst. Although the axial GaAs/InAs NW heterostructures have been reported earlier,[13,14] no detailed investigation of the GaAs/InAs heterointerfaces were given, though this information is important.

In this letter, we use transmission electron microscopy (TEM) to investigate detailed structural and compositional characteristics of the GaAs/InAs and InAs/GaAs interfaces. From experiment results, the NW evolutions through GaAs/InAs and InAs/GaAs heterointerfaces are determined.

GaAs/InAs and InAs/GaAs NW heterostructures were grown in a horizontal flow low pressure (100 mbars) metal-organic chemical vapor deposition reactor using 30 nm size Au nanoparticles dispersed on $(111)_B$ GaAs substrates and at a growth temperature of 450 °C. For GaAs/InAs NW heterostructures, InAs NWs were first grown for 30 min under trimethylindium (TMI) and AsH_3 flow. GaAs NW sections were then grown on top of these InAs NWs for 3 or 30 min by switching off the TMI flow and switching on the trimethylgallium (TMG) flow, while maintaining a constant AsH_3 flow. After the GaAs growth, the growth chamber was cooled to 350 °C under AsH_3 pressure. In a similar way, InAs/GaAs NW heterostructures were produced by growing InAs NW sections for 1 min on the 30 min grown GaAs NWs. The flow rates of TMI, TMG, and AsH_3 were 1.2×10^{-5}, 1.2×10^{-5}, and 5.4×10^{-4} mol/min, respectively. Scanning electron microscopy (SEM) (JEOL 890) and transmission electron microscopy [FEI Tecnai F20 equipped with scanning transmission electron microscope (STEM) and an energy dispersive spectrometer (EDS)] investigations were carried out. TEM specimens were prepared by gently touching the as-grown substrates against TEM grids.

Figure 1(a) shows a typical SEM image of GaAs/InAs NW heterostructures in which the majority of NW heterostructures have grown vertically to the substrate surface, i.e., along the $\langle111\rangle_B$ direction. In order to identify the GaAs/InAs interface, STEM and EDS characterizations were conducted on individual NW heterostructures. Figure 1(b) shows a STEM dark-field image of a typical GaAs/InAs NW heterostructure, where GaAs and InAs sections and the Au nanoparticle can be distinguished by their different contrasts. Figure 1(c) shows the EDS line scan across the GaAs/InAs interface of the NW heterostructure. To minimize the arti-

a)Authors to whom correspondence should be addressed. Electronic addresses: j.zou@uq.edu.au and chennupati.jagadish@anu.edu.au.

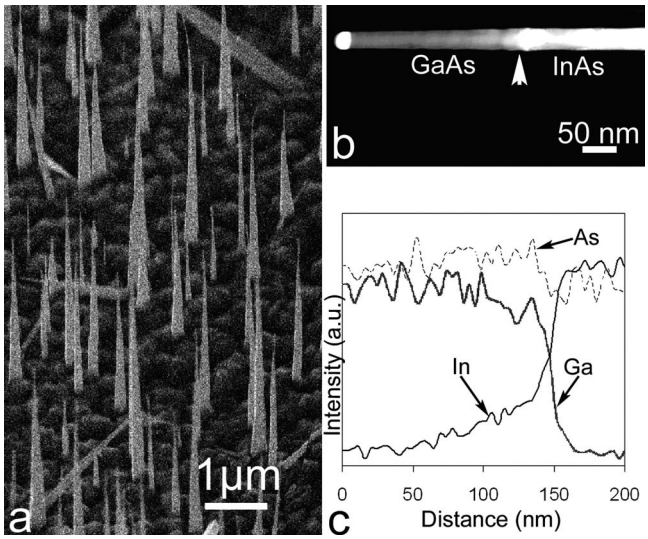

FIG. 1. (a) SEM image of GaAs/InAs NW heterostructures (3 min grown GaAs) grown on a GaAs (111)B substrate; (b) and (c) are STEM image of a GaAs/InAs NW heterostructure (3 min grown GaAs) and its corresponding EDS line scan at the interface region respectively.

facts in the EDS measurements, the NWs were orientated nearly perpendicular to the EDS detector. As shown in Fig. 1(c), the GaAs/InAs interface is not sharp in terms of the composition. In fact, it shows a transition region of InGaAs (for a length of ~50–70 nm within the EDS detectability) after the InAs segment (from right to left). EDS analysis shows that the In composition decreases gradually in the InGaAs segment and followed by the GaAs segment.

In order to verify the atomic structures of the GaAs/InAs interfaces, high resolution (HR) TEM was conducted. Figure 2(a) shows a typical TEM image of the top section of a chosen InAs/GaAs NW heterostructure in which the GaAs/InAs interface and the catalyst can be seen. Figure 2(b) is the corresponding HRTEM image at the interface region in which the wurtzite structure is followed by many stacking faults along the NW growth direction. These stacking faults decrease significantly after ~50 nm along the NW growth direction followed by the zinc-blende structure, as shown in Fig. 2(c). To understand the strain relaxation around the interface, fast Fourier transformation (FFT) was performed around the interface region and the result is shown in Fig. 2(d). If a sharp interface exists between InAs and GaAs, there should be clearly distinguishable diffraction spots present in the FFT pattern, even with the presence of the stacking faults in the interface region. As can be seen from Fig. 2(d), however, the appearance of the diffraction bands [an enlarged example is shown in the inset of the Fig. 2(d)] indicates that the interface between GaAs and InAs is not sharp. In order to determine the position of the GaAs/InAs interface and its compositional variation around the interface, we carefully measured the interatomic distances on the {0001} or {111} planes that are perpendicular to the NW growth direction. The distance between 40 atoms (to minimize the measurement error) in each atomic plane was measured and plotted in terms of the percentage of the lattice misfit along the NW growth direction, as presented in Fig. 2(e). Based on this analysis, the GaAs/InAs interface can be determined and marked in Fig. 2(b). In order to verify the lattice distortions around the interface, we also measured the interplanar spacings of the {0001} or {111} planes that are

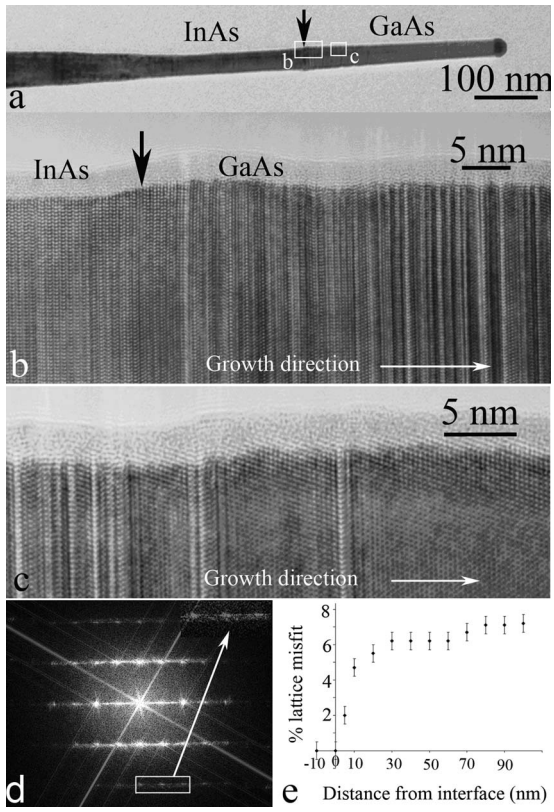

FIG. 2. (a) and (b) are TEM image of a GaAs/InAs NW heterostructure (3 min grown GaAs) and HRTEM image at the GaAs/InAs interface region respectively. (c) HRTEM image showing the significant reduction in stacking faults in the GaAs NW section. (d) FFT image taken at the interface region and the inset shows a magnified image of some of diffraction spots. (e) Plot of lattice misfit between the lattice spacings along the GaAs/InAs interface.

perpendicular to the NW growth direction and obtained similar results as shown in Fig. 2(e). This similarity of the lattice relaxation in both *in-plane* and *axial* directions indicates no significant lattice distortions in these heterostructures. These results suggest that no sharp GaAs/InAs interface exists, and, in fact, the majority of the lattice misfit has been relieved gradually along the NW growth direction over a distance of ~50–70 nm. Such a gradual change is possibly due to the incorporation of In in the GaAs segment during its growth, in agreement with the EDS measurements [Fig. 1(c)].

To understand the fundamental reasons for this blurred GaAs/InAs NW interface (i.e., GaAs growth on InAs NW sections), we examine the reverse case, that is, the InAs/GaAs NW interfaces. Figure 3(a) shows a TEM image of the top region of a typical InAs/GaAs NW heterostructure, where the InAs nucleates at an edge of the Au-alloy/GaAs interface. This occurs to minimize the interfacial area between the Au-alloy particle and the InAs segment.[7] Figure 3(b) is the corresponding high-resolution TEM (HRTEM) image showing the InAs/GaAs interface and its FFT pattern is shown in Fig. 3(c). Two sets of diffraction spots can be clearly seen. By careful analysis of the FFT pattern and HRTEM images, the InAs/GaAs interfaces are determined to be atomically sharp.

To understand why GaAs growth on InAs resulted in a diffuse GaAs/InAs interface and why the InAs growth on GaAs resulted in a sharp InAs/GaAs interface, we note that the NW growth is led by the Au catalysts, and therefore, we

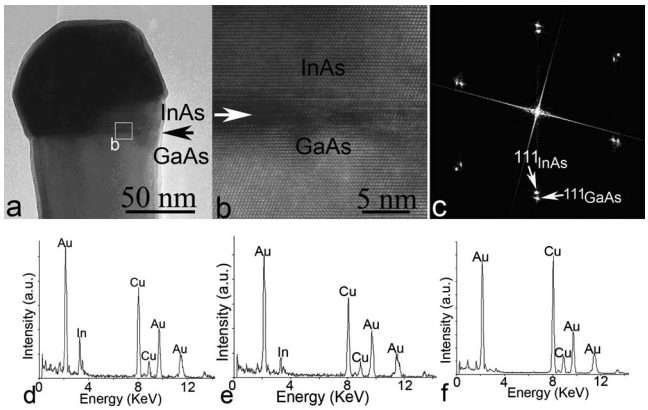

FIG. 3. (a) TEM image of tip region of an InAs/GaAs NW (1 min InAs grown on GaAs NW), and (b) is the corresponding HRTEM image of the InAs/GaAs interface region with its FFT image in (c). (d)–(f) are the EDS spot analyses of Au particles at different stages of GaAs/InAs NWs growth: (d) no GaAs growth, (e) and (f) after GaAs NWs growth for 3 and 30 min, respectively.

must determine the difference in the interactions of group III elements with the Au catalysts. To understand this difference, we measured the compositions of catalysts at different growth stages of GaAs on InAs NW sections, that is, GaAs NW growth for 0 (no GaAs growth), 3, and 30 min, respectively. Figures 3(d)–3(f), respectively, show typical EDS measurements of catalysts in these three cases. In the case of purely InAs NWs (no GaAs growth), the In concentration in the catalysts is measured as ~21 at. %, whereas, in the case of GaAs NWs growth for 3 min, the In concentration is ~10 at. % and in the case of 30 min GaAs growth, almost no In was detected in catalysts. It should be noted that, after growth termination and during cooling, Ga may be released from the catalyst particles and reacts with ambient As vapor species to form GaAs.[12,15] In the case of InAs NWs (cooled under As vapor species), In was found inside the Au catalysts.[16] Even in the case of InGaAs NWs (cooled under As vapor species), Ga was released and only In was detected in the Au catalysts after the cooling .[17]

The composition variations shown in Figs. 3(d)–3(f) suggest that the In originally in the catalysts is released during the GaAs growth, so that the InGaAs transition segment must be due to the incorporation of released In into the GaAs NW segment. When the Au–In catalysts are exposed to Ga vapor, Ga will incorporate into the Au–In catalysts, and consequently, the Au–In–Ga catalysts form. Our estimation shows that the In content in InGaAs transition region is much higher than the difference between the In content of the solidified Au catalysts after the InAs NW growth and after 3 min GaAs NW growth [Figs. 3(d) and 3(e)]. Therefore, after InAs NW growth, the Au–In alloy catalyst should have contained much more In than that detected in the solidified catalyst [Fig. 3(d)]. In the reverse case, the atomically sharp InAs/GaAs interface suggests that the Ga in the Au catalyst is fully released before the onset of InAs growth, i.e., when the Au–Ga alloyed catalysts are exposed to the In vapor, the catalysts quickly change their composition from Au–Ga to Au–In by simultaneously absorbing In and expelling Ga.

In the case of GaAs/InAs heterointerface, In tends to remain within the Au-alloyed catalysts even under the Ga vapor. In contrast, in the case of InAs/GaAs heterointerface, Ga is expelled from the catalysts quickly under the In vapor. These differences suggest that In might have more thermodynamic affinity toward Au than Ga during NW growth,[18] resulting in the sharp InAs/GaAs interface. It is of interest to note, from Fig. 3(e), that In was detected in the Au catalysts even after 3 min growth of GaAs, and, as shown in Fig. 1(c), this 3 min GaAs growth resulted in an InGaAs transition segment followed by a GaAs section. The In variation in the solidified Au–In catalysts before and after the GaAs growth [Figs. 3(d) and 3(e)] can be qualitatively used to explain the generation of the InGaAs segment. During the initial stage of GaAs growth, a significant amount of In in the liquid catalyst is released and incorporated in the GaAs segment until a relatively steady composition is established in the catalyst.[11] The fact that In is released during the GaAs growth suggests that kinetics also plays a role.[19] As seen from Fig. 3(f), no In is detected in the catalyst after 30 min growth of GaAs, suggesting that even after the balanced composition is reached in the catalyst, In is still released from the catalysts. We expect that this release of In would also incorporate in GaAs NW sections, but this In concentration is beyond the EDS detection limit. As shown in Figs. 2(b) and 2(c), the InAs section is followed by a high density of stacking faults and then these stacking faults decrease significantly, and then NW growth continues with a zinc-blende structure. We believe that these stacking faults occur due to instabilities at the NW/catalyst interface during the initial growth of GaAs, and this may be related to the compositional changes occurring within the Au catalysts.

In conclusion, we have investigated the nature of heterointerfaces of GaAs/InAs and InAs/GaAs axial NW heterostructures. We observed the diffuse GaAs/InAs heterointerface and the atomically sharp InAs/GaAs heterointerface. These interesting observations demonstrate that, in the growth of axial NW heterostructures, the difference in interaction between catalyst particles and the elements diffusing through the catalyst play a critical role in the final abruptness of the heterointerfaces of axial NW heterostructures.

The Australian Research Council was acknowledged for the financial support of this project.

[1]H. J. Fan, P. Werner, and M. Zacharias, Small **2**, 700 (2006).
[2]S. Perera *et al.*, Appl. Phys. Lett. **93**, 053110 (2008).
[3]A. J. Mieszawska *et al.*, Small **3**, 722 (2007).
[4]N. Wang, Y. Cai, and R. Q. Zhang, Mater. Sci. Eng., R. **60**, 1 (2008).
[5]R. S. Wagner and W. C. Ellis, Appl. Phys. Lett. **4**, 89 (1964).
[6]B. E. Sundquist and L. F. Mondolfo, Trans. Metall. Soc. AIME **221**, 157 (1961).
[7]M. Paladugu *et al.*, Small **3**, 1873 (2007).
[8]K. A. Dick *et al.*, Nano Lett. **7**, 1817 (2007).
[9]M. Paladugu *et al.*, Appl. Phys. Lett. **91**, 133115 (2007).
[10]Y. N. Guo *et al.*, Appl. Phys. Lett. **89**, 231917 (2006).
[11]T. E. Clark *et al.*, Nano Lett. **8**, 1246 (2008).
[12]A. I. Persson *et al.*, Nat. Mater. **3**, 677 (2004).
[13]B. J. Ohlsson *et al.*, Physica E (Amsterdam) **13**, 1126 (2002).
[14]K. Hiruma *et al.*, J. Cryst. Growth **163**, 226 (1996).
[15]J. C. Harmand *et al.*, Appl. Phys. Lett. **87**, 203101 (2005).
[16]K. A. Dick *et al.*, Nano Lett. **5**, 761 (2005).
[17]D. Sudfeld *et al.*, Phase Transitions **79**, 727 (2006).
[18]K. A. Dick *et al.*, Adv. Funct. Mater. **15**, 1603 (2005).
[19]S. Kodambaka *et al.*, Science **316**, 729 (2007).